# Revisiting the Hydration of Pb(II): A QMCF MD Approach

**Anirban Bhattacharjee,[†] Thomas S. Hofer,[†] Andreas B. Pribil,[†] Bernhard R. Randolf, Len Herald V. Lim,[†] Andreas F. Lichtenberger,[‡] and Bernd M. Rode*,[†]**

*Theoretical Chemistry Division, Institute of General, Inorganic and Theoretical Chemistry, University of Innsbruck, Innrain 52a, A-6020 Innsbruck, Austria, and Technical College HTL Anichstrasse, Innsbruck Anichstrasse, A-6020 Innsbruck, Austria*

*Received: June 22, 2009; Revised Manuscript Received: August 13, 2009*

A quantum mechanical charge field (QMCF) molecular dynamics (MD) study of Pb(II) in an aqueous medium was carried out in order to gain insight into its solvation behavior, for both structural and dynamic aspects. Applying the advanced methodology and different basis sets, some new aspects concerning the solvation of Pb(II) have been revealed. One of the most interesting outcomes of the current simulation is the variation of first shell coordination number from 7 to 9 in the $Pb(H_2O)_n^{2+}$ complex with $Pb(H_2O)_8^{2+}$ as a major species. Moreover, a far more dynamic and labile hydration shell was found compared to previous QM/MM MD simulation with only the first hydration shell treated by quantum mechanics, which reported a very rigid first hydration shell with a fixed coordination number of 9. The current simulation results are in much better agreement with the properties reported from the recent thermodynamic studies than the previous QM/MM MD study.

## 1. Introduction

Lead, the heaviest member of the 14th group, is a potent toxin, although it has been widely used for various industrial processes,[1] leading to the issue of "lead pollution". The most stable aqueous species of lead is the Pb(II) cation; although the Pb(IV) species exists in solution, it is highly oxidizing in nature. To our knowledge, no neutron diffraction investigations were reported for hydrated Pb(II) ion and extensive absorption of X-rays by Pb[2] is also a problem for carrying out X-ray diffraction experiments. The first theoretical approach to describe Pb(II) in aqueous solution was a QM/MM MD simulation study including the ion and its first shell in the QM region,[3] which led to a very rigid first solvation shell without any ligand exchange. However, considering the large ionic radius of Pb(II) (1.19 Å),[4] this behavior was quite surprising. A recent thermodynamic analysis of Pb(II) hydration reported an 8-fold 8 coordination to be favored by the first hydration shell,[5] and it was concluded that formation of coordination numbers 6−8 is almost thermoneutral.[5] In contrast to this, the one shell QM/MM MD[3] has reported a first shell coordination number value of 9 for the whole simulation span and no first shell ligand exchange was observed.[6] This finding also contrasts with the experimentally determined value of the water exchange rate between the primary and secondary hydration shells, which was reported as $1 \times 10^9$ $s^{-1}$.[7] Considering these ambiguities, a new study of the hydration of Pb(II) appeared highly desirable with application of the advanced QMCF MD methodology,[8−10] which also includes the second hydration shell in the QM treatment at the *ab initio* level. In addition, a classical simulation was also performed with a pair potential and threebody correction, which enabled the study of exchange events over a long time span (2 ns) and solvation effects at different temperatures.

* Corresponding author. E-mail: Bernd.M.Rode@uibk.ac.at. Phone: +43-512-507-5161. Fax: +43-512-507-2714.
[†] University of Innsbruck.
[‡] Technical College HTL Anichstrasse.

## 2. Methods

In the QMCF approach like in other QM/MM methodologies,[11−14] the system of interest is divided into two parts: the chemically most important region, which is treated by a quantum mechanical technique, and the remaining part of the system described by means of classical mechanics. This procedure proved efficient to describe complex electronic effects and polarization taking place near the solute. However, unlike in the conventional QM/MM framework, the QMCF approach does not require solute−solvent potentials.[8,9] This is of particular advantage as the construction of these potential functions is a delicate, time-consuming, and sometimes difficult task. It was observed during QM/MM MD simulations of hydrated ions that non-Coulombic interactions between solute and solvent become negligibly small at a distance of a few angstroms after which all significant interactions result from Coulombic contributions. Therefore, as long as the solute resides at the center of the QM region and the radius of the QM region remains sufficiently large, only the Coulombic interactions between the solute and the MM solvent molecules need to be evaluated. Solvent particles close to the center, videlicet inside the core zone (i.e., the first shell ligands of an ion), can be treated in the same way, whereas for solvent molecules located close to the QM/MM border, namely, the layer zone, both non-Coulombics and Coulombics have to be evaluated, as the interatomic distances are short. This concerns, however, only solvent−solvent interactions for which the same potential can be applied as for MM particles. Thus, the second QM region (layer) consisting of only solvent molecules increases the accuracy of the simulation and enables the description of the intershell processes. The point charges of all MM particles (in accordance with the respective MM model) are included in the core Hamiltonian as a perturbation potential to obtain a more realistic description of the influence of surrounding solvent molecules on the quantum mechanical region. This charge embedding technique has been applied in various methods to polarize the QM region.[15−17] Otherwise artifical surface effects may result, as the QM region

10.1021/jp905848x CCC: $40.75 
Published on Web 09/03/2009

**TABLE 1: Average Binding Energies in kcal/mol for Pb(II)−$(H_2O)_n$ Clusters of Different Size Obtained from HF, MP2, CCSD, and B3LYP Calculations**

| *n* | HF | MP2 | CCSD | B3LYP |
|---|---|---|---|---|
| 1 | −61.36 | −61.49 | −61.69 | −69.62 |
| 2 | −53.66 | −53.73 | −53.92 | −59.97 |
| 3 | −53.76 | −50.36 | −54.04 | −59.00 |
| 4 | −49.62 | −49.68 | −49.87 | −53.52 |
| 5 | −46.35 | −46.37 | −46.57 | −49.29 |
| 6 | −43.35 | −43.31 | −43.52 | −46.29 |
| 8 | −37.68 | −37.61 | | −39.49 |

**TABLE 2: Average Pb−O Distances in Å for Pb(II)−$H_2O$ Clusters of Different Size Obtained from HF, MP2, CCSD, and B3LYP Calculations**

| *n* | HF | MP2 | CCSD | B3LYP |
|---|---|---|---|---|
| 1 | 2.37 | 2.34 | 2.36 | 2.34 |
| 2 | 2.51 | 2.47 | 2.48 | 2.47 |
| 3 | 2.45 | 2.41 | 2.42 | 2.42 |
| 4 | 2.52 | 2.47 | 2.49 | 2.5 |
| 5 | 2.58 | 2.53 | 2.54 | 2.57 |
| 6 | 2.66 | 2.59 | 2.61 | 2.61 |
| 8 | 2.78 | 2.70 | | 2.72 |

resides in an artificial vacuum environment and, hence, is unaware of the existence of the bulk molecules. Because of the varying positions of the MM point charges along the simulation, the QM region is embedded in a continuously fluctuating field of charges.[8,9] In addition to that, discontinuities of forces may take place when a solvent molecule enters or leaves the QM region (because of the difference in the definition of forces in the two regions), so a special treatment is performed whenever solvent molecules leave and enter the QM region. In order to ensure a continuous change of forces, a smoothing function is applied in the distance 5.9−6.1 Å from the center. Further details of the QMCF methodology have been published elsewhere.[8,9]

The partial charges assigned to the MM particles employed for embedding were taken in accordance with the BJH−CF2 water model[18,19] which was utilized to describe the MM water molecules throughout the simulation. These charges are −0.65966 and 0.32983 unit charges for oxygen and hydrogen, respectively. The partial charges for the atoms inside QM regions were obtained using Mulliken population analysis,[20,21] as it has been found to yield partial charges for the QM particles in the layer region that proved compatible with the charges assigned to the MM particles..[22,23]

An important aspect is the choice of basis set, balancing computational effort and accuracy. On the basis of ion−water cluster calculations, we have chosen the cc-PVDZ-pp basis set for Pb(II)[24] and DZP(Dunning) for hydrogen and oxygen.[25] As described earlier in this Article, the cc-pVDZ-PP basis set with a smaller 60 electron ECP[26] was chosen to achieve a higher accuracy in the electronic structure calculation, while the aug-cc-pVDZ-PP basis set with the same number of core electrons was chosen for the most recent study in this case.[5] However, the cluster calculations in both cases yield similar geometrical parameters and bonding energies differing in the range 0.1−0.2%, so the smaller size basis set (cc-pVDZ-PP) was chosen over the larger one (aug-cc-pVDZ-PP) in order to reduce the computation time in the QMCF procedure.

We also performed cluster calculation for $[Pb-(H_20)_{1-8}]^{+2}$ clusters with different methods including HF, B3LYP, MP2, and CCSD. The results are listed in Tables 1 and 2.

These results also indicate effects of electron correlation and many-body effects to be expected during the simulation. As can be observed from Table 1, the average hydration energy values differ slightly (less than even 0.5 kcal/mol) for HF, MP2, and CCSD, but the difference is quite considerable in the case of B3LYP. However, neither MP2 nor CCSD is computationally affordable for simulation at present, so we prefer to use HF as the level of theory for the QM calculation. The BSSE (basis set superposition error) calculations were also performed for the Pb(II)−monohydrate at different levels of theory and were included in Table 3. The data indicates that BSSE and electron correlation do not have any significant contribution for the system of interest.

**TABLE 3: Basis Set Superposition Error According to the Boys−Bernardi Procedure for Pb(II)−$H_2O$ Obtained from HF, MP2, CCSD, and B3LYP Calculations**

| BSSE (in kcal/mol) | |
|---|---|
| HF | 0.78 |
| MP2 | 3.11 |
| CCSD | 2.97 |
| B3LYP | 1.68 |

The simulation of one Pb(II) in a 1000 water box was started at 298.15 K, using the Berendsen algorithm for thermostatization;[27] the long-range Coulombics were accounted for by the reaction field method. The time step used for the simulation was 0.2 fs, and trajectories were recorded every fifth step. The radius of the core region was taken as 3.5 Å, and that of the layer region as 6.1 Å. Smoothing[8,9] was applied between 5.9 and 6.1 Å to ensure a continuous transfer of solvent molecules between the QM and MM regions.

Prior to the QMCF simulation, a classical MD simulation was performed not only in order to obtain a suitable starting configuration but also to study ligand exchange dynamics over a large time span and at different temperatures. The classical simulations have been performed applying the same potential used as in a previous QM/MM MD simulation[3] with one Pb(II) in a 1000 water box. Similar as in the QMCF MD simulation, the Berendsen algorithm has been used for thermostatization[27] and the reaction field correction was used for handling long-range Coulombics. The sampling was performed for 2 ns, with a time step of 0.2 fs. The trajectories were recorded after every 100 steps.

In addition to the structural information, the most important dynamical properties, such as mean residence time of ligand molecules and the ion−oxygen stretching frequency were also evaluated. The velocity autocorrelation function (VACF) $C(t)$ provides direct insight into the dynamics of a fluid system, as the time integrals are related to macroscopic transport coefficients and the Fourier transformations are related to the vibrational spectra.

$$C(t) = \frac{\sum_{i}^{N_t}\sum_{j}^{N} \vec{v}_j(t_i)\vec{v}_j(t_i + t)}{N_t N \sum_{j}^{N} \vec{v}_j(t_i)\vec{v}_j(t_i)} \quad (1)$$

The spectrum was obtained using eq 1, where $N$ is the number of particles, $N_t$ is the number of time origins $t_i$, and $\vec{v}_j$ denotes a specific velocity component of the $j$th particle. The power spectrum of the VACF was obtained by a Fourier transformation using a correlation length of 2.0 ps and averaging over 2000 time origins. Approximate normal coordinate analysis[28] was used to obtain the vibrational frequencies. No scaling factor[29,30] was

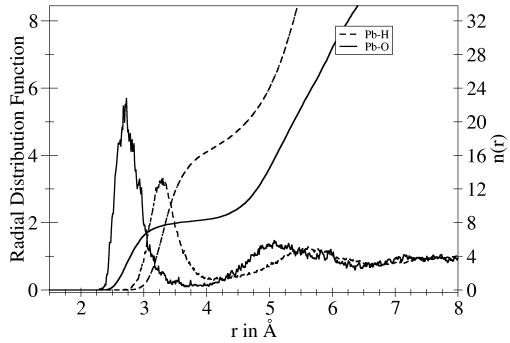


**Figure 1.** Pb−O (solid line) and Pb−H (dashed line) radial distribution functions and their running integration numbers.

applied. In order to obtain detailed insight into ligand exchange processes, mean residence time (MRT) values were calculated by the direct method,[31] using eq 2.

$$\tau = \frac{t_{\mathrm{sim}}\mathrm{CN}_{\mathrm{av}}}{N_{\mathrm{ex}}} \tag{2}$$

where $\tau$ is the mean residence time, $t_{\mathrm{sim}}$ is the simulation time, $\mathrm{CN}_{\mathrm{av}}$ the average coordination number, and $N_{\mathrm{ex}}$ the number of exchanges with a minimum displacement time of $t^* = 0.5$ ps.[32] In case no exchange events are observed during the simulation, a lower limit of the MRT can be estimated using eq 3.

$$\tau \geq \tau_{\mathrm{limit}} = t_{\mathrm{sim}} \cdot \mathrm{CN}_{\mathrm{av}} \tag{3}$$

In addition, the sustainability of the ligand exchange process can be measured by comparing the number of transitions through a shell boundary ($N_{\mathrm{ex}}^{0}$) to the number of events lasting at least 0.5 ps ($N_{\mathrm{ex}}^{0.5}$). Using this, a sustainability coefficient for exchange has been defined as[31]

$$S_{\mathrm{ex}} = N_{\mathrm{ex}}^{0.5}/N_{\mathrm{ex}}^{0} \tag{4}$$

The inverse of $S_{\mathrm{ex}}$ (i.e., $R_{\mathrm{ex}} = 1/S_{\mathrm{ex}}$) defines how many border crossing attempts are required to achieve one successful exchange (spanning over at least $t^* = 0.5$ ps).[31]

## 3. Results and Discussion

The Pb−O radial distribution function (depicted in Figure 1) shows two well-defined hydration shells in agreement with the previous QM/MM simulation,[3] but the peak intensities are quite different: the previous study had shown a far more rigid structure, while the current simulation indicates a relatively labile hydration. The details of the current and previous simulation are summarized in Table 4. Differing from the previous QM/MM MD simulation, the first and second hydration shells are not so well separated and the second hydration shell is much broader, as seen from the Pb−O radial distribution function. This is basically the consequence of the many-body polarization effect and charge transfer due to its inclusion in the QM region instead of using fixed point charges for the solvent molecules in the second shell. The difference in the first shell structure (shifting of the first peak from 2.60 to 2.72 Å) is probably an adjustment to the improved description of its immediate surrounding. The usage of a different basis set with a smaller ECP could have had some minor effect, too, because the average

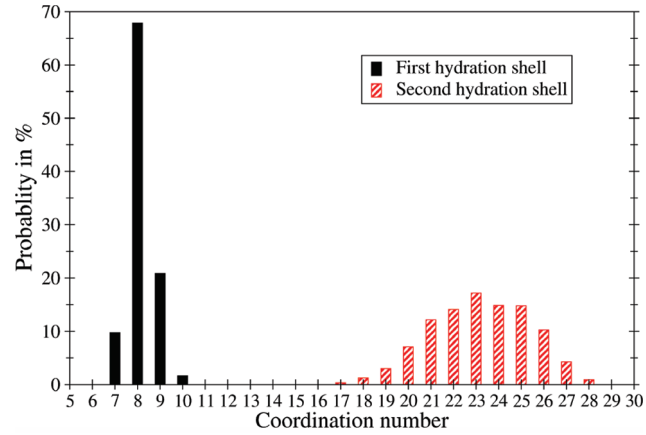


**Figure 2.** Coordination number distribution for the first and second shell of Pb(II) cation.

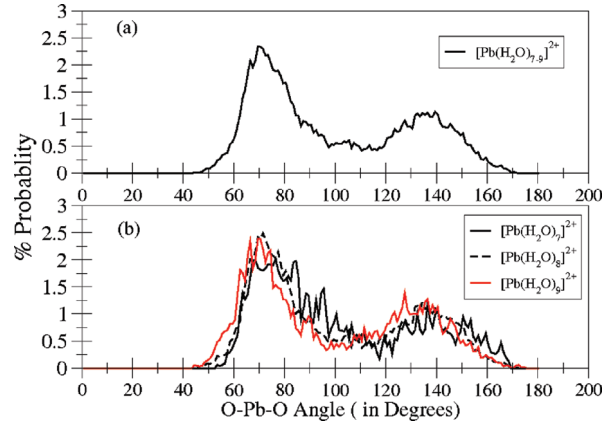


**Figure 3.** O−Pb−O angle distribution plots for the first hydration shell of Pb(II): (a) for the entire trajectory; (b) for configurations with 7-, 8-, and 9-fold coordinated lead−aquo complexes.

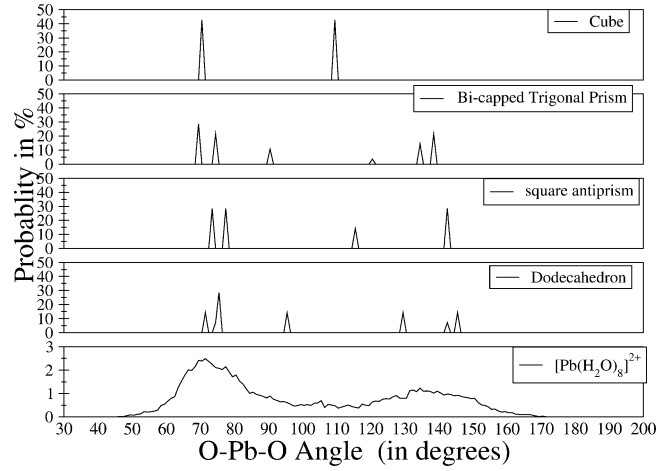


**Figure 4.** O−Pb−O angle distribution plots for the first hydration shell of $Pb(H_2O)_8^{2+}$ and that of standard geometries for 8 coordinated species.

Pb−O distances obtained from the gas phase hydrate cluster geometry optimizations using the current basis set (cc-pVDZ-PP) are also slightly larger (see Table 2) than those obtained using SBKJC VDZ ECP.[3] However, the border region of this shell does not differ much; the minimum is found at 3.68 Å in the QMCF simulation and 3.65 in the previous QM/MM MD study.[3] The Pb−H radial distribution function also shows two peaks, the first peak appearing at 3.32 Å and the second peak at 5.61 Å (in the previous simulation,[3] 3.25 and 5.35 Å,

**TABLE 4: Maxima $r_M$ and Minima $r_m$ of the Radial Distribution Function in Å and Average Coordination Number of the Respective Shells from the Present Simulation and the Previous QM/MM MD Simulation[3]**

| | $r_{M1}$ | $r_{m1}$ | $r_{M2}$ | $r_{m2}$ | $CN_{av,1}$ | $CN_{av,2}$ |
|---|---|---|---|---|---|---|
| Current Simulation | | | | | | |
| Pb−O | 2.72 | 3.68 | 5.07 | 6.375 | 8.1 | 25.3 |
| Pb−H | 3.32 | 4.0 | 5.61 | 6.74 | 16.2 | 56.2 |
| QM/MM MD Simulation[3] | | | | | | |
| Pb−O | 2.60 | 3.65 | 5.0 | 5.9 | 9.0 | 24.3 |
| Pb−H | 3.25 | 4.0 | 5.35 | 6.4 | 18.0 | 57.6 |
| Classical MM/MD Simulation (This Work) | | | | | | |
| Pb−O (at 25 °C) | 2.70 | 3.70 | 5.12 | 6.13 | 9.0 | 26.6 |
| Pb−O (at 95 °C) | 2.73 | 3.69 | 4.93 | 5.61 | 9.0 | 20.8 |

respectively). The results from the classical MD simulation which has been obtained using a pair potential and a three-body correction[3] at two different temparatures (25 and 95°) have also been included in Table 4. The position of the first peak of the Pb−O radial distribution function obtained is close to that obtained from the QMCF simulation (2.69 and 2.72 Å, respectively), but the first shell coordination number resulting from the classical simulation is 9, identical to the QM/MM MD value. The second shell maxima and respective upper boundaries listed in Table 4 match neither with the QM/MM MD nor with the QMCF simulation, but the differences are small enough to use the long classical trajecory for further comparison. One interesting fact observed from the classical simulation is that the first shell coordination number does not change when moving from 25 to 95 °C, which indicates the hydrate is still stable near the boiling point of water. The decrease in the distance of the upper boundary and the coordination number of the second shell at higher tempareture (as can be seen from Table 4) indicates the partial breakdown of the second shell structure which is expected at a fairly high temperature.

In order to obtain further information concerning the structural entities, the coordination number distributions were calculated for the first and second solvation shells (*cf.* Figure 2). The differences between the QMCF and the QM/MM simulation[3] become clearly visible. Unlike the exclusive first shell coordination number of 9 throughout the whole QM/MM simulation, the coordination number of the system now varies in the range 7−10 with a major contribution from $Pb(H_2O)_8^{2+}$ (62.4%), followed by $Pb(H_2O)_9^{2+}$ (19.2%), then $Pb(H_2O)_7^{2+}$ (16.9%), and a rare occurrence of $Pb(H_2O)_{10}^{2+}$ (1.5%). Recent calculations by Clark et al.[5] lead to the conclusion that formation of coordination number 6−8 is all almost thermoneutral, with $Pb(H_2O)_8^{2+}$ being the coordination number favored for the first hydration shell. However, the referred work predicted the results based on gas phase cluster calculations and therefore cannot really reflect the equilibrium situation in solution at a finite temperature.

So far, with the help of RDF (radial distribution function) and CND (coordination number distribution), we have derived at the quanitative description of different hydration layers. However, none of these describes the spatial arrangement of the water ligands in the first hydration shell. The microstructure of the first shell can be primarily investigated by the calculation of angular distribution functions (ADFs) for the O−Pb−O angle (as depicted in Figure 3a). The overall ADF for the first shell consists of contributions mainly from microstructures of 7-fold to 9-fold coordinated species. Configurations from the trajectory with different first shell coordination numbers were then extracted, and the respective O−Pb−O ADFs were calculated for each set of configurations. These plots are shown in Figure 3b.

Apparently, the distributions are wide, indicating a large number of exchanges passing through intermediate geometries. According to the present work, the 8-fold coordinated species appears to be the major species, and thus, we compared its angular distribution function with that of standard 8-fold coordinated geometries (illustrated in Figure 4). The presence of any cubic geometries can be immediately excluded. Some resemblance in the distribution is observed for the square antiprism structure, which is the reported structure from optimization.[5] However, some similarity in the distribution also exists for the dodecahedron and/or the bicapped trigonal prism. It can be concluded that, therefore, for the major hydrate, the spatial distributions of the eight water oxygen atoms around the ion can assume three regular geometries—bicapped trigonal prismatic, square anti prismatic, and dodecaheral (as depicted in Figure 5a, b, and c, respectively)—but also that in most of the configuration slight distortions from the exact geometries occur due to the dynamics associated with rapid ligand exchanges. The effect of the lone electron pair which is observed for the lower members of divalent ions of group IV (Ge(II)[33] and Sn(II)[34]) is not pronounced in the case of Pb(II); at most, it produces merely slight distortions of the first hydration shell structure.

Another interesting aspect to observe from the simulation is the relative orientation of the water ligands which provides further insight into the hydration behavior. The relative orientation of these ligands is characterized by two angular parameters, one being $\theta$, the angle between the Pb−O vector, and the vector resulting from the sum of the O−H vectors and the tilt angle, which is defined as the angle between the Pb−O vector and the plane defined by the O−H vectors. Tilt and $\theta$ angle distributions are depicted in Figure 6a and b. The distributions of the tilt angle show a broad peak spanning between ±85°

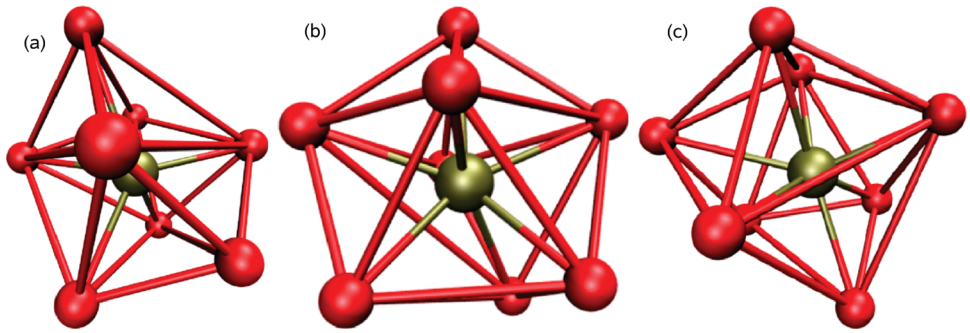


**Figure 5.** Different geometries, close to the regular polyhedral structures observed for distribution of water oxygens around the Pb(II) ion similar to (a) a bicapped trigonal prism, (b) a square antiprism, and (c) a dodecahedron.

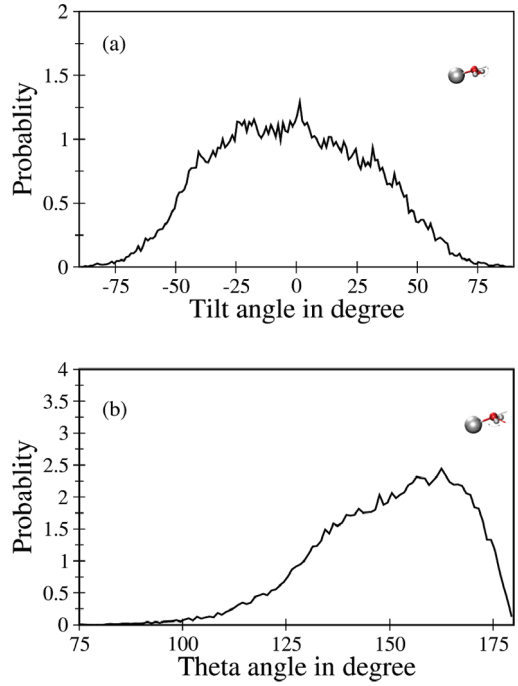


**Figure 6.** (a) Tilt and (b) $\theta$ angle distributions of the Pb(II)−$H_2O$ geometry.

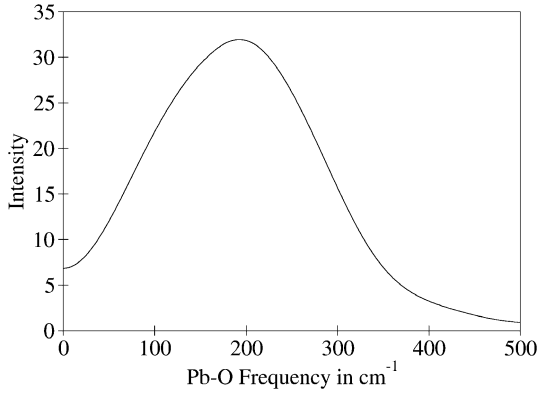


**Figure 7.** Power spectrum in cm$^{-1}$ of the Pb(II)−O stretching mode in the first hydration shell.

with a maximum at 0° (slightly broader than the QMM/MM MD simulation result[3]). The distribution of the tilt angle is very similar to Ba(II)[35] which is expected because of its comparable size-to-charge ratio. The $\theta$ angle, starting from 81° and peaking at ∼162°, is also broader than that obtained from the previous simulation, where it is starting from 95°, with a peak at 160°.[3] The $\theta$ distribution is also similar to that obtained for Ba(II) cation,[35] showing a maximum at ∼155° and significant tailing toward 85°. However, the $\theta$ angle distributions differ significantly from other divalent cations such as Ca(II),[36] Cu(II),[37] Co(II),[38] and Hg(II).[39] However, it is similar to that of large monovalent hydrated cations like Au(I)[40] and Ag(I),[41] reflecting an increased flexibility of the gearing of the aquo groups around the ion. The broader distributions of both tilt and $\theta$ angles point toward a higher degree of orientational flexibility of the system compared to the QM/MM MD simulation.

The power spectrum of the Pb(II)−O vibrational mode is displayed in Figure 7. The average frequency of the Pb(II)−O stretching motion is 196 cm$^{-1}$ and the calculated force constant is 33.6 N/m, very similar to those of Ba(II) (200 cm$^{-1}$ and 33.8 N/m).[35] There is a considerable difference from the previous QM/MM MD,[6] where the Pb(II)−O first shell stretching frequency was found as 217 cm$^{-1}$ with a corresponding force constant of 37.4 N/m. This difference indicates that the quantum mechanical treatment of first and second shell and other methodical improvements of the QMCF MD approach are crucial for a reliable description of the stability/lability of a hydrated ion.

One particular advantage of simulation methods is the access to the position of all atoms and their time evolution, enabling the characterization of ultrafast ligand exchange dynamics occurring in both the first and second hydration shells. The overview of different dynamical parameters has been given in Table 5 including the comparison with the previous QM/MM MD study.[6] The results from classical MD simulations at 25 and 95 °C have also been included using the available pair potential and three-body correction terms[3] (as shown in Table 5).

One of the most interesting outcomes of the current simulation is the observed first shell exchanges leading to a $\tau^{0.0}$ value of 2.07 ps and a $\tau^{0.5}$ value of 5.53 ps, as no such event was reported for the previous QM/MM MD simulation.[6] The QMCF MD simulation leads to a sustainability coefficient $S_{ex}$ value of 0.38 and a corresponding $R_{ex}$ value of 2.7. This appears to be more reasonable because of its comparibility with the heavy metal cations Hg(II)[31] and Ba(II),[35] having $R_{ex}$ values of 2.9 and 2.5, respectively. The classical MD simulation shows exchanges in the first hydration shell both at normal and elevated temperature. The classical MD simulation spanning over a large time scale (2 ns) yields a $\tau^{0.0}$ value of 10.9 ps and a $\tau^{0.5}$ value of 230 ps, which signifies a rather rigid first hydration shell. However, unlike the QM/MM MD simulation, the classical simulation shows first shell ligand exchange processes, which is certainly due to the much longer simulation period than that of the QM/MM MD simulation. The ratio of the MRT values for exchanges exceeding 0.5 ps at 25 °C for the classical and the QMCF MD simulation is around 42. Dividing the MRT value obtained at 95 °C from the classical simulation by this ratio allows a simple extrapolation of the MRT value from QMCF at that temperature

**TABLE 5: Mean Residence Time $\tau$ in ps, Number of Accounted Ligand Exchange Events $N_{ex}$ per 10 ps, and Sustainability of the Migration Process $S_{ex}$ to/from the First and Second Hydration Shell for a $t^*$ Value of 0.0 and 0.5 ps**

| | $N_{ex}^0$/10 ps | $\tau^{0.0}$ | $N_{ex}^{0.5/10ps}$ | $\tau^{0.5}$ | $S_{ex}$ | $R_{ex}(1/S_{ex})$ |
|---|---|---|---|---|---|---|
| | | First Shell | | | | |
| present work | 38.5 | 2.07 | 14.44 | 5.53 | 0.375 | 2.7 |
| QM/MM MD[3] | no exchange reported | | | | | |
| | | Classical MM/MD | | | | |
| at 25 °C | 8.21 | 10.9 | 0.4 | 229.18 | 0.049 | 20.41 |
| at 95 °C | 10.19 | 8.83 | 0.99 | 93.37 | 0.097 | 10.30 |
| | | Second Shell | | | | |
| present work | 481.5 | 0.48 | 109.8 | 2.1 | 0.23 | 4.38 |
| QM/MMMD[3] | 386 | 0.63 | 43 | 5.6 | 0.11 | 9.0 |

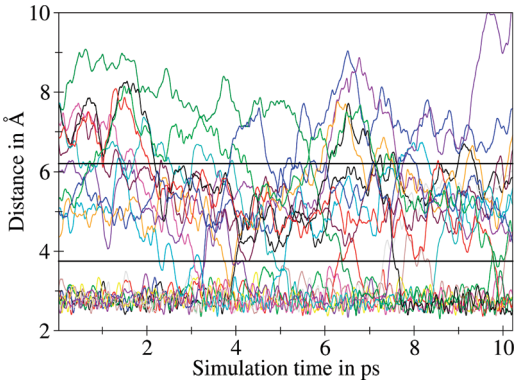


**Figure 8.** Pb(II)−O distance plot of first shell ligands depicting ligand migrations between different solvation shells.

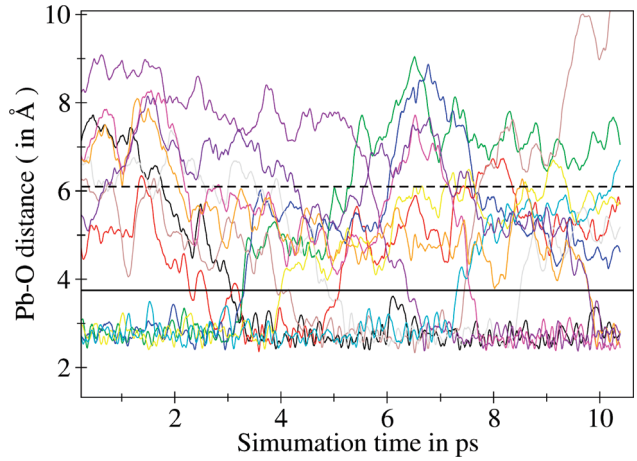


**Figure 9.** Pb(II)−O distance plot of the first shell ligands which have undergone successful exchanges spanning over 0.5 ps. The straight horizontal line depicts the first shell boundary, and the dashed one indicates the second shell upper boundary.

to 2.25 ps. This can be safely assumed to be the lower limit of the real MRT value, and it is still larger than that of water (1.2 ps obtained from QMCF MD simulation). This indicates that even at the elevated temperature 95 °C the Pb(II) cation still retains its structure forming ability.

The mean ligand residence time for the second shell for a $t^*$ value of 0.5 ps obtained form the current simulation is 2.1 ps, and $R_{ex}$ is 4.38. The $R_{ex}$ value is considerably lower than the previous value of 9.0, signifying that a lesser number of border crossing events is necessary to produce one successful exchange, again indicating a far more labile second hydration shell, compatible with the large size of the Pb(II) ion. As can be seen from Table 5, the classical MD simulation yields results that resemble more those of the one shell QMM/MM MD as expected.

Figure 8 displays the distance plots of the first shell ligands; the shell borders have also been specified with straight horizontal lines. The exchange events are clearly visible from the plot. It appears that only two of the first ligands remained throughout the whole simulation, and three of them exchanged for a short time and returned. All remaining ligands either exchanged permanently or carried out at least one exchange spanning more than 0.5 ps.

The nature of ligand exchanges taking place in the first hydration shell can be perceived by looking at the Pb−O distance plot of the sustainably exchanged water ligands which is depicted in Figure 9.

The basic nature of the ligand exchanges is associative, resulting in a higher coordination number which becomes more likely because of the large size of the ion which enables it to accommodate more water ligands in its vicinity. The associations are not always immediately followed by the leaving of another first shell ligand, which can be delayed for more than 0.5 ps. An interesting case of a ligand interchange is visible from the plot around 2.6 ps simulation time where the entry and departure of water ligands take place almost simultaneously.

## 4. Conclusion

The work presented here has provided an advanced insight into the hydration of Pb(II) covering structural as well as dynamical characteristics of the ion. A relatively labile first hydration shell with multiple coordination number possibilities and ultrafast ligand exchange are the most important differences from the previous studies performed by conventional QM/MM MD technology. Using the accuracy of the *ab initio* QMCF MD simulation as the control and scaling that for much faster classical MD allowed the application of the latter to estimate elevated temperature effects, showing that Pb(II) still retains its structure forming ability near the boiling point of water.

**Acknowledgment.** Financial support from the Austrian Science Foundation (FWF) is gratefully acknowledged.

## References and Notes

(1) Da Silva, J. R. F.; Williams, R. J. P. *The Biological Chemistry of Life*; Clarendon: Oxford, U.K., 1991.
(2) Ohtaki, H.; Radnai, T. *Chem Rev.* **1993**, *93*, 1157.
(3) Hofer, T. S.; Rode, B. M. *J. Chem. Phys.* **2004**, *121*, 6406.
(4) Shannon, R. D. *Acta Crystallogr.* **1976**, *751*, A32.
(5) Wander, M. C. F.; Clark, A. E. *Inorg. Chem.* **2008**, *47*, 8233.
(6) Hofer, T. S.; Randolf, B. R.; Rode, B. M. *Chem. Phys.* **2006**, *323*, 473.
(7) Stumm, W.; Morgan, J. J. *Chemical equilibria and rates in natural waters*, 3rd ed.; Wiley-Interscience: New York, 1985; p 77.
(8) Rode, B. M.; Hofer, T. S.; Randolf, B. R.; Schwenk, C.; Xenides, D.; Vchirawongkwin, V. *Theor. Chem. Acc.* **2006**, *115* (2−3), 77.
(9) Rode, B. M.; Hofer, T. S.; Randolf, B. R.; Pribil, A. B.; Vchirawongkwin, V. In *Trends and Perspectives in Modern Computational Science*; Maroulis, G., Simos, T., Eds.; International Science Publishers (VSP): Leiden, The Netherlands, **2006**, 441−442.
(10) Hofer, T. S.; Pribil, A. B.; Randolf, B. R. *Pure Appl. Chem.* **2008**, *80* (6), 1195.
(11) Warshel, A.; Levitt, M. *J. Mol. Biol.* **1976**, *103*, 227.
(12) Field, M. J.; Bash, P. A.; Karplus, M. *J. Comput. Chem.* **1990**, *11* (6), 700.
(13) Gao, J. *J. Am. Chem. Soc.* **1993**, *115*, 2930.
(14) Bakowies, D.; Thiel, W. *J. Phys. Chem.* **1996**, *100* (25), 10580.
(15) Lin, H.; Truhlar, D. G. *Theor. Chim. Acta* **2007**, *117*, 185.
(16) Laio, A.; VandeVondele, J.; Rothlisberger, U. *J. Chem. Phys.* **2002**, *116*, 6941.
(17) Voloshina, E.; Gaston, N.; Paulus, B. *J. Chem. Phys.* **2007**, *126*, 134115.
(18) Stillinger, F. H.; Rahman, A. *J. Chem. Phys.* **1978**, *68* (2), 666.
(19) Bopp, P.; Janscó, G.; Heinzinger, K. *Chem. Phys. Lett.* **1983**, *98* (2), 129.
(20) Mulliken, R. S. *J. Chem. Phys.* **1955**, *23* (10), 1833.
(21) Mulliken, R. S. *J. Chem. Phys.* **1955**, *23* (10), 1841.
(22) Hofer, T. S.; Randolf, B. R.; Rode, B. M. *J. Phys. Chem. B* **2008**, *112* (37), 11726.
(23) Hofer, T. S.; Randolf, B. R.; Rode, B. M. *Phys. Chem. Chem. Phys.* **2005**, *7*, 1382.
(24) Peterson, K. A. *J. Chem. Phys.* **2003**, *119*, 11099.
(25) Dunning, T. H., Jr. *J. Chem. Phys.* **1970**, *53* (7), 2823.
(26) B. Metz, B.; Stoll, H.; Dolg, M. *J. Chem. Phys.* **2000**, *113*, 2563.
(27) Berendsen, H. J. C.; Postma, J. P. M.; van Gunsteren, W. F.; DiNola, A.; Haak, J. R. *J. Chem. Phys.* **1984**, *81* (8), 3684–3690.
(28) Bopp, P. *Chem. Phys.* **1986**, 106.
(29) Scott, A. P.; Radom, L. *J. Phys. Chem.* **1996**, *100*, 16502.
(30) DeFrees, D. J.; McLean, A. D. *J. Chem. Phys.* **1985**, *82*, 333.
(31) Hofer, T. S.; Tran, H. T.; Schwenk, C. F.; Rode, B. M. *J. Comput. Chem.* **2004**, *25*, 211.

(32) Lock, A. J.; Woutersen, S.; Bakker, H. J. *Femtochemistry and Femtobiology*; World Scientific: Singapore, 2001.
(33) Azam, S.; Hofer, T. S.; Randolf, B. R.; Rode, B. M. *Chem. Phys. Lett.* [Online early access]. DOI: 10.1016/j.cplett.2009.01.041. Published Online: Jan 20, **2009**.
(34) Lim, L. H. V.; Hofer, T. S.; Randolf, B. R.; Pribil, A. B.; Rode, B. M. *J. Phys. Chem. B* **2009**, *113*, 4372.
(35) Hofer, T. S.; Randolf, B. R.; Rode, B. M. *Chem. Phys.* **2005**, *312*, 81.
(36) Schwenk, C. F.; Lffler, H. H.; Rode, B. M. *J. Chem. Phys.* **2001**, *115*, 10808.
(37) Schwenk, C. F.; Rode, B. M. *ChemPhysChem* **2003**, *4*, 931.
(38) Armunanto, R.; Schwenk, C. F.; Setiaji, A. H.; Rode, B. M. *Chem. Phys.* **2003**, *295*, 63.
(39) Kritayakornupong, C.; Plankensteiner, K.; Rode, B. M. *Chem. Phys. Lett.* **2003**, *371*, 438.
(40) Armunanto, R.; Schwenk, C. F.; Tran, H. T.; Rode, B. M. *J. Am. Chem. Soc.* **2004**, *126*, 2582.
(41) Armunanto, R.; Schwenk, C. F.; Rode, B. M. *J. Phys. Chem. A* **2003**, *107*, 3132.

JP905848X